Simulation of Double Fed Induction Generator Wind Power System

[1]A. Sharath kumar, [2]G. Akhila, [3]T. Sravya
[1]Assistant professor, [2]Graduate student, [3]Graduate student
[1]Department of Electrical and Electronics Engineering,
Kamala Institute of Technology & Secience, Telangana, India.

_____

Abstract - This paper describes the basic performance of a wind power system based on induction generator. The induction machine which is taken for the purpose of study is the doubly fed induction generator (DFIG). The techniques of direct grid integration, independent power control, and the droop phenomenon of distribution line are studied for DFIG systems. System is modelled in MAT lab/Simulink environment and results are observed for various wind speeds of the turbine.

Index Terms—Doubly fed induction machines, field-oriented control, maximum power tracking, wind power system.

_____

I. INTRODUCTION

The Increasing emphasis on renewable wind energy has given rise to augmented attention on more reliable and advantageous electrical generator systems. Induction generator systems have been widely used and studied in wind power system because of their advantages over synchronous generators, such as smaller size, lower cost, and lower requirement of maintenance [1], [2].

The doubly fed induction generator (DFIG) with variable-speed ability has higher energy capture efficiency and improved power quality and thus has attracted more attentions. With the advent of power electronic techniques, a back-to-back converter, which consists of two bidirectional converters and a dc link, acts as an optimal operation tracking interface between generator and grid [3]–[5]. Field-oriented control (FOC) is applied to both rotor- and stator-side converters to achieve desirable control on voltage and power [6], [7]. Generally, the FOC has been presented based on DFIG mathematical equations only. However, a three-phase choke is commonly used to couple the stator-side converter into the grid. Therefore, this paper proposes the FOC schemes of stator-side converter involving the choke, and it turns out that both stator- and rotor side converter voltages consist of a current regulation part and a cross-coupling part.

In this paper the modelling and simulation DFIG wind system is studied. The paper is organized as follows. The wind turbine is modelled and simulated using the turbine emulator, and an expression of optimal output power versus rotor speed is proposed in Section 2. In Section 3, the DFIG is introduced by mathematical model in Section 4, indicating the relationship of voltage, flux, and torque. At last, simulation results are presented and discussed in Section 5.

II. WINDTURBINE

Wind energy is extracted through wind turbine blades and then transferred by the gearbox and rotor hub to the mechanical energy in the shaft, which drives the generator to convert the mechanical energy to electrical energy. The turbine model is based on the output power characteristics, expressed as [3], [8]

$$P_m = C_p(\lambda, \beta) \cdot \frac{1}{2} \rho A v_w^3 \tag{1}$$

$$\lambda = \frac{R_{\text{blade}} \omega_r}{v_w} \tag{2}$$

Where P_m is the mechanical output power in watts, which depends on power performance coefficient C_p, air density ρ, turbine swept area A, and wind speed Vw.$(1/2) \cdot \rho A v^3{}_w$ is equal to the kinetic energy contained in the wind at a particular speed Vw. The performance coefficient $C_p(\lambda, \beta)$, which depends on tip speed ratio λ and blade pitch angle β, determines how much of the wind kinetic energy can be captured by the wind turbine system. A nonlinear model describes $C_p(\lambda, \beta)$ as [8]
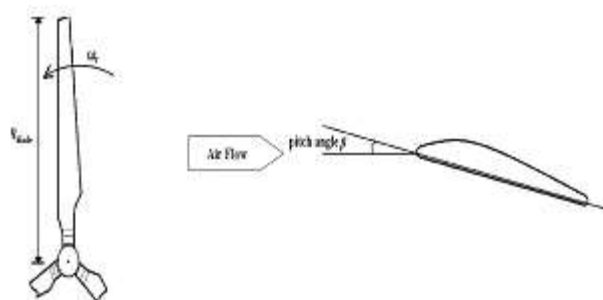
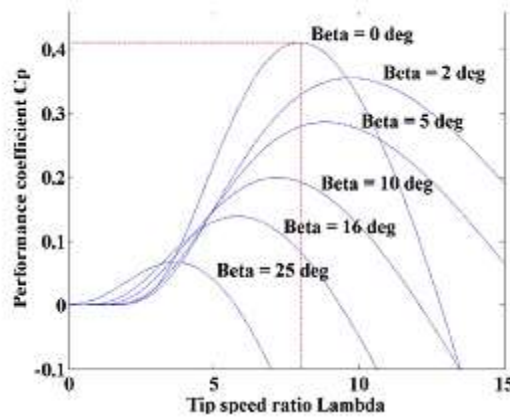

Fig-1: Schematics of turbine blade from different views

Fig-2: $C_p{-}\lambda$ curve for the turbine model

$$C_p(\lambda, \beta) = c_1(c_2 - c_3\beta - c_4\beta^2 - c_5)e^{-c_6} \tag{2}$$

where c_1=0.5, c_2= 116/λ_i, c_3=0.4, c_4=0, c_5=5, c_6=21/λ_i, and

$$\frac{1}{\lambda_i} = \frac{1}{\lambda + 0.08\beta} - \frac{0.035}{\beta^3 + 1} \tag{3}$$

Where R_{blade} and ω_r are the blade radius and angular frequency of rotational turbine as depicted in Fig.1. The $C_p{-}\lambda$ curve for this particular turbine model at different β is shown in Fig. 2 where it is illustrated that, to achieve maximum Cp, one has β=0∘ and λ=8. The blade with fixed geometry will have fixed $C_p{-}\lambda$ characteristics, as described in (2) and(3). Therefore, to track the optimal output power, the curve of $P_m{-}\omega_r$ is the "map" to follow.

In order to experimentally investigate the operation of wind turbine, a wind turbine emulator system is built to operate in torque control mode, using (1a)

$$T = \frac{P}{\omega_r} = \frac{1}{2}\rho\pi R_{blade}^3 v_w^2 \frac{C_p}{\lambda} = \frac{1}{2}\rho\pi R_{blade}^3 v_w^2 C_m \tag{4}$$

Where C_m is the torque performance coefficient. It is dependent on on ω_r, v_w, and β. Thus, based on turbine $C_p{-}\lambda$ model and by assuming β=0∘,the $C_m{-}\lambda$ curve is given in Fig. 3. At any particular v_w, one could obtain different torque and, thus, power output by varying rotor speed. The system configuration is shown in Fig. 4, where the ω_r is fed back to the controller for calculating C_m and, then, torque command.
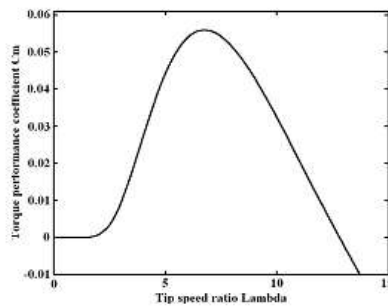

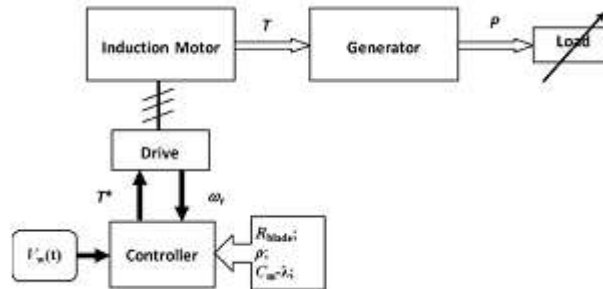**Fig-3:** $C_m{-}\lambda$ curve for the turbine emulator

Fig-4: Wind turbine emulator system.
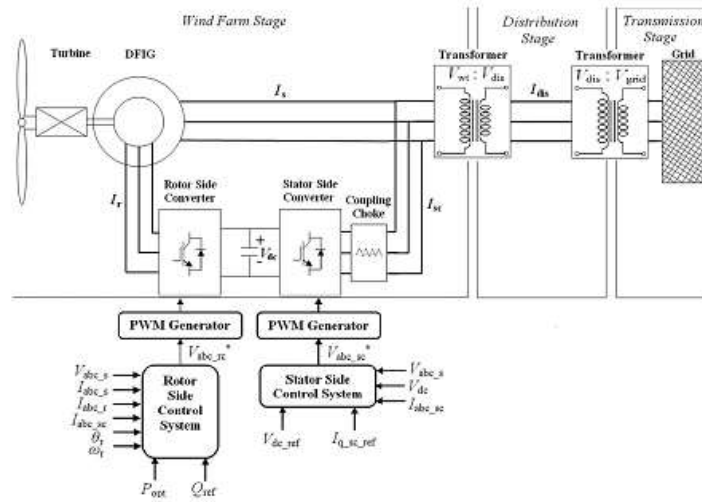
III. DFIG WIND POWER SYSTEM

Fig-5: Wind turbine–doubly fed induction generator system configuration.

Traditionally, the dynamic slip control is employed to fulfil the variable-speed operation in wind turbine system, in which the rotor windings are connected to variable resistor and control the slip by the varied resistance [3], [10]. This type of system can achieve limited variations of generator speed, but external reactive power source is still necessary. Consequently, to completely remove the reactive power compensation and to control both active and reactive power independently, DFIG wind power system is one of most popular methods in wind energy applications [1], [3], [7]. This paper reproduces DFIG model first of all and then concentrates on the controlling schemes of power converters, in which the active and reactive power are controlled independently. In particular, the stator-side converter control involving an RL series choke is proposed. Both controlling of rotor- and stator side converter voltages end up with a current regulation part and a cross-coupling part. The wind turbine driving DFIG wind power system consists of a wound-rotor induction generator and an ac/dc/ac insulated gate bipolar transistor (IGBT)-based pulse width-modulated (PWM) converter (back-to-back converter with capacitor dc link), as shown in Fig. 5. In this configuration, the back-to-back converter consists of two parts: the stator-/grid-side converter and the rotor-side converter. Both are voltage source converters using IGBTs, while a capacitor between two converters acts as a dc voltage source. The generator stator windings are connected directly to grid (with fixed voltage and frequency of grid) while the rotor winding is fed by rotor-side converter through slip rings and brushes, at variable frequency.

The control system is divided into two parts—stator-side converter control system and rotor-side converter control system. An equivalent circuit of DFIG is depicted in Fig. 6, and the relation equations for voltage V, current I, flux Ψ, and torque Te involve [4], [11], [12] are:

$$V_{ds} = R_s I_{ds} - \omega_s \Psi_{qs} + \frac{d\Psi_{ds}}{dt}$$

$$V_{qs} = R_s I_{qs} + \omega_s \Psi_{ds} + \frac{d\Psi_{qs}}{dt}$$

$$\qquad (5)$$

$$V_{dr} = R_r I_{dr} - s\omega_s \Psi_{qr} + \frac{d\Psi_{dr}}{dt}$$

$$V_{qr} = R_r I_{qr} + s\omega_s \Psi_{dr} + \frac{d\Psi_{qr}}{dt}$$

$$\qquad (6)$$

$$\Psi_{ds} = L_s I_{ds} + L_m I_{dr}$$

$$\Psi_{qs} = L_s I_{qs} + L_m I_{qr}$$

$$\qquad (7)$$

$$\Psi_{dr} = L_r I_{dr} + L_m I_{ds}$$

$$\Psi_{qr} = L_r I_{qr} + L_m I_{qs}$$

$$\qquad (8)$$

$$T_e = \frac{3}{2} n_p (\Psi_{ds} I_{qs} - \Psi_{qs} I_{ds})$$

$$\qquad (9)$$

Where $L_s = L_{ls} + L_m$; $L_r = L_{lr} + L_m$; $s\omega_s = \omega_s - \omega_r$ represents the difference between synchronous speed and rotor speed; subscripts r, s, d, and q denote the rotor, stator, d-axis, and q-axis components, respectively; T_e is electromagnetic torque; and L_m, n_p, and J are generator mutual inductance, the number of pole pairs, and the inertia coefficient, respectively.
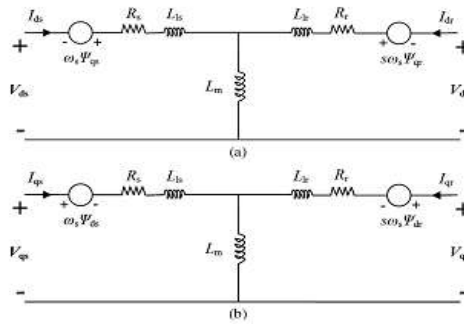
Fig- 6: Equivalent circuit of DFIG. (a)d-axis model. (b)q-axis model

A. Rotor-Side Converter Control

If the derivative parts in (5) are neglected, one can obtain stator flux as

$$\Psi_{ds} = (V_{qs} - R_s I_{qs})/\omega_s$$

$$\Psi_{qs} = (V_{ds} - R_s I_{ds})/(-\omega_s)$$

$$\Psi_s = \sqrt{\Psi_{ds}^2 + \Psi_{qs}^2}.$$ (10)

Because of being directly connected to the grid, the stator voltage shares constant magnitude and frequency of the grid. One could make the d-axis align with stator voltage vector; it is true that $V_s = V_{ds}$ and $V_{qs} = 0$, thus $\Psi_s = \Psi_{qs}$ and $\Psi_{ds} = 0$, which is of stator-voltage-oriented vector control scheme, as
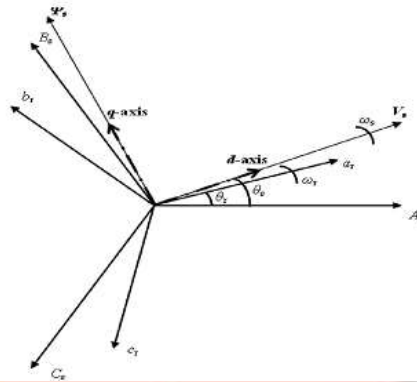

Fig-7: Stator voltage FOC reference frame.

depicted in Fig. 7. According to (7)–(9), the rotor-side converter reference current is derived as

$$I_{dr\_ref} = -\frac{2L_s T_e}{3n_p L_m \Psi_s}$$ (11)

Where

$$P_{e\_ref} = P_{opt} - P_{loss} = T_e \omega_r$$

$$P_{loss} = R_s I_s^2 + R_r I_r^2 + R_c I_{sc}^2 + F\omega_r^2$$ (12)

Where I_{sc}, R_c, and Fare stator-side converter current, choke resistance, and friction factor, respectively. P_{opt}, P_{e_ref}, and Ploss are desired optimal output active power, reference active power, and system power loss. Combining (10)–(12), the active power is used as command inputs to determine current reference I_{dr_ref}. Meanwhile, the output reactive power is the stator reactive output power since the stator-side converter's reactive power is set to be zero. Then, one has
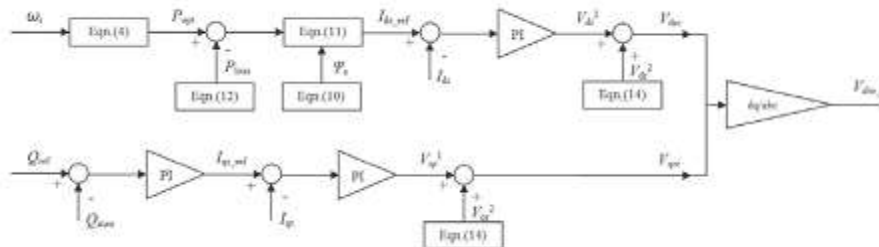

Fig-8: Rotor-side converter control scheme

$$Q_o = Q_s + Q_{sc} = Q_s = \text{Im}\left[(V_{ds} + jV_{qs})(I_{ds} + jI_{qs})^*\right] - V_s I_{qs} - V_{ds}\frac{1}{L_s}(\Psi_s - L_m I_{ds})$$ (13)

Thus, the regulation of reactive power can lead toI_{qr_ref}, and then, the rotor-side converter voltage signals V_{1dr}andV_{1qr} are derived by the regulation of currents. In addition, the feed forward coupling partsV_{2dr} and$V_{2qr}$are derived based on (6) and(8), as

$$V_{dr}^2 = R_r I_{dr} - s\omega_s(L_r I_{qr} + L_m I_{qs})$$

$$V_{qr}^2 = R_r I_{qr} + s\omega_s(L_r I_{dr} + L_m I_{ds})$$

(14)

where the superscripts 1 and 2 denote the current regulation part and cross-coupling part, respectively. At last, rotor-side converter voltage signals in dq-axes are expressed as

$$V_{drc} = V_{dr} = V_{dr}^1 + V_{dr}^2$$

$$V_{qrc} = V_{qr} = V_{qr}^1 + V_{qr}^2$$

(15)

where subscript rc denotes the rotor-side converter. After the conversion of dq−abc, the rotor-side converter voltage V_{abc_rc} can be obtained. Fig. 8 exhibits the control scheme for the aforementioned procedure.

B. Stator-Side Converter Control

Concerning the use of three-phase series RL choke between stator- and stator-side converter, a cross-coupling model is required to derive the voltage signal of stator-side converter, as described in Fig. 9

$$V_{dsc} = V_{ds} - V_{dch}$$

$$V_{qsc} = V_{qs} - V_{qch}$$

(16)

where the subscri ptssc and chde note the variables of stator side converter and choke. The coupling part of voltage signals V_{dch}^2 and V_{qch}^2 is expressed as

$$V_{dch}^2 = R_c I_{dsc} - \omega_s L_c I_{qsc} \;,\; V_{qch}^2 = R_c I_{qsc} + \omega_s L_c I_{dsc}$$
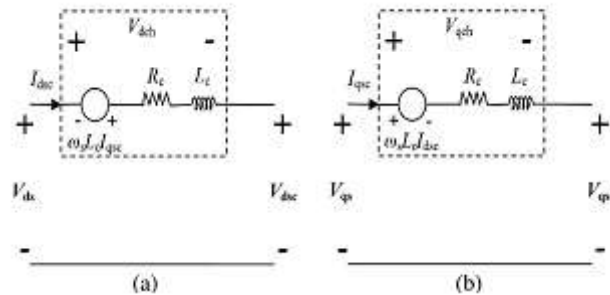
(17)

Fig-9: Equivalent circuit of stator-side-converter choke. (a)d-axis model. (b)q-axis model.

Moreover,V_{dch}^1 andV_{qch}^1 are determined by the regulation of currents I_{ds} c and I_{qsc} in which the current reference Iqsc_ref is given directly while I_{dsc_ref} is determined by the regulation of dc-link voltage V_{dc}. Thus, above all, the stator-side converter voltage signals V_{dsc} and V_{qsc} are obtained as follows and depicted in Fig. 10:

$$V_{dsc} = V_{ds} - V_{dch}^1 - V_{dch}^2$$

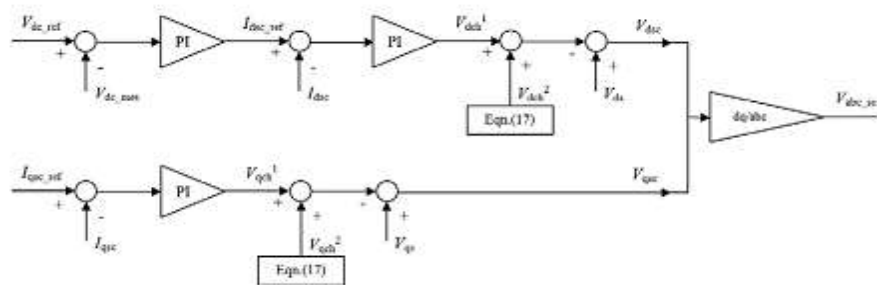$$V_{qsc} = V_{qs} - V_{qch}^1 - V_{qch}^2$$

(18)

Fig-10: Stator-side converter control scheme.

IV. SIMULATION ANALYSIS AND RESULTS

A. DFIG

By using the proposed optimal power curve as well as the system parameters listed in Table I, the DFIG wind power system is simulated. The DFIG system allows the optimal (maximum) output power operation in the absence of reactive power source. Also, the independent control of active and reactive power is achieved. In the Matlab/Simulink model, the converter switch frequency is set to be 27 times the grid frequency f. To achieve acceptable accuracy, the power circuit and the control circuit models are discretized at different time steps. It is worthy to note that the nominal apparent power and nominal active power are considered as nominal electrical power and nominal mechanical power in this wind power system [3], [13]. Simulation and control system parameters are listed in Table II.
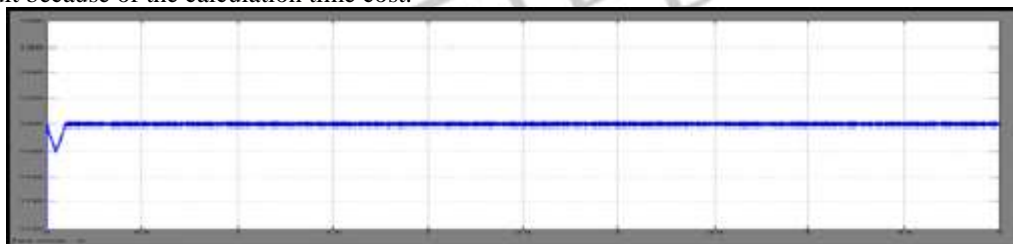
Table-I
DFIG-BASED WIND POWER SYSTEM PARAMETERS

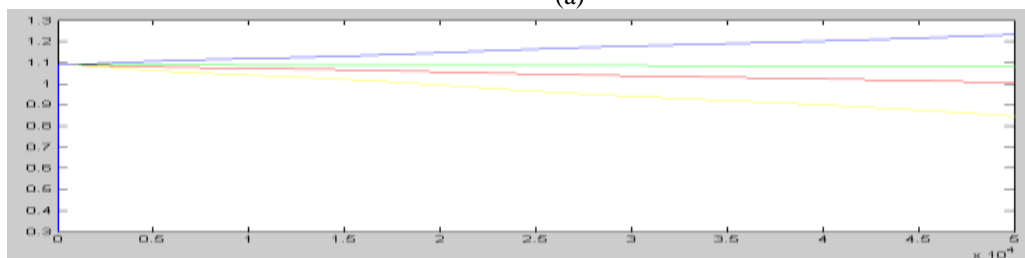| Parameter	Value
Nominal Wind Speed v_w	11 m/s
Nominal Apparent Power S_e	1.67 MVA
Nominal Active Power P_{nDFIG}	1.5 MW
Power Factor pf	0.9
Grid Voltage V_{grid}	120 kV
Grid Frequency f	60 Hz
Distribution Line Voltage V_{dis}	12.5 kV
Wind Turbine Bus Voltage V_{wt}	575 V
Generator Number of Pole Pairs n_p	3
Stator Resistance R_s	0.0071 p.u.
Stator Leakage Inductance L_s	0.171 p.u.
Referred Rotor Resistance R_r	0.005 p.u.
Referred Rotor Leakage Inductance L_r	0.156 p.u.
Stator-to-Grid Coupling Resistance R_c	0.003 p.u.
Stator-to-Grid Coupling Inductance L_c	0.3 p.u.
Mutual Inductance L_m	2.9 p.u.
Nominal DC-link Voltage V_{dc}	1.2 kV
DC-link Capacitance C	10 mF
Maximum C Converter Current I_{conv_max}	0.5 p.u.
System Inertia Coefficient H	5 second
Generator Friction Damping F	0.01 p.u.

Table-II
SIMULATION AND CONTROL PARAMETERS

Parameter	Value
Power System Sampling Period T_{s_Power}	5e-6 sec
Control System Sampling Period $T_{s\_Control}$	1e-4 sec
Switch Frequency f_{sw}	1620 Hz
Transmission Distance D_{tran}	30 km
Reactive Power Regulator Coefficients K_p; K_i	0.05; 5
DC-link Voltage Regulator Coefficients K_p; K_i	0.002; 0.1
Rotor-side Current Regulator Coefficients K_p; K_i	0.3; 8
Stator-side Current Regulator Coefficients K_p; K_i	2.5; 500

First of all, the steady-state results of the system are shown in Fig. 11(a)–(d), where four wind speed cases Vw= 7,9,10, and12m/s to verify the optimal power output tracking are presented. All of them kept the bus voltage at 1200 Vdc, indicating the well operation of stator-side converter, while the reactive power is set to be zero as the input command. In order to track the optimal active power output, optimal rotor speeds are implemented accordingly. Similarly, the optimal trackings of output power and rotor speed are exhibited in other wind speed cases as well. Therefore, it can be concluded that the system works well to follow the optimal power control at steady-state operation. It is noticed that P and Q are vanished during the first cycle (1/60 s) in displayed result because of the calculation time cost.
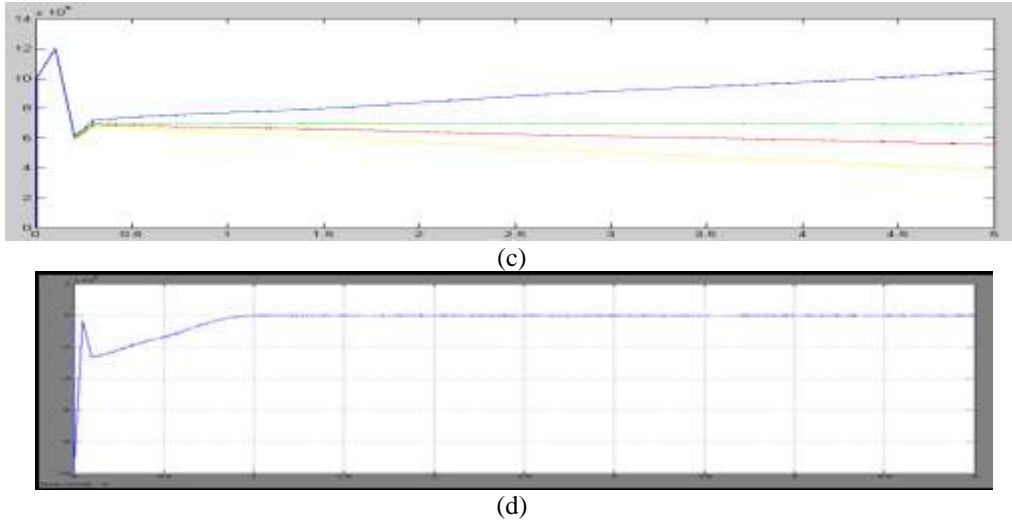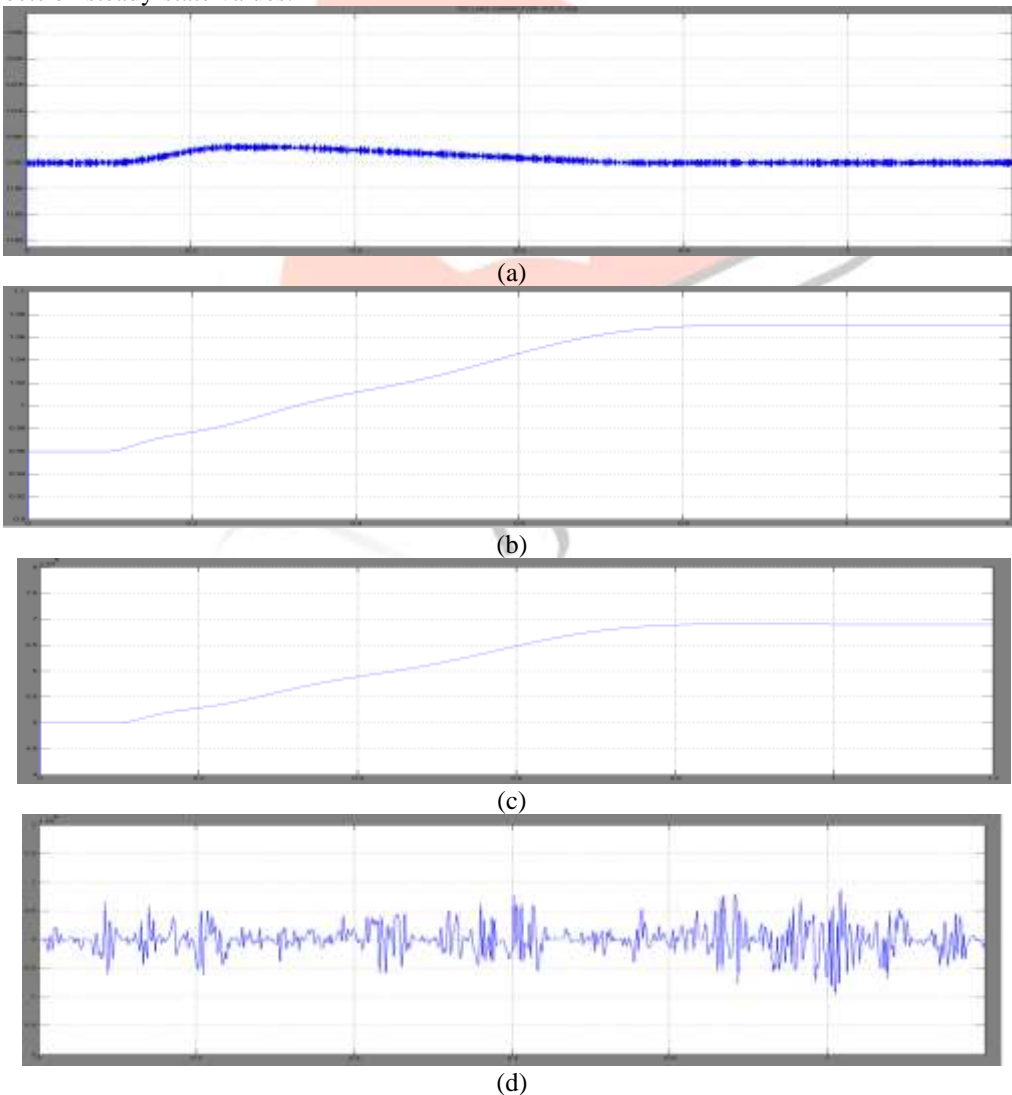

(a)

(b)

(c)

(d)

Fig-11: System responses to different constant wind speeds. (a) DC-link voltage V_{dc}. (b) Rotor speed ω_r. (c) Active power P. (d) Reactive power Q

Second, the system dynamic response to varied wind speeds is investigated. Due to the large H of the system, dynamic variation can last and be observed in a long time period before converging to the steady-state values. To shorten such period, H=0.1s is used in this part of simulation. With stable steady-state initial values, three regular types of wind speeds are examined for dynamic responses, including step, ramp, and gusty winds. The varied winds and corresponding results for Vdc, ω_r, P, and Q are shown in Figs. 11, where the system can always reach a new optimal steady state after a few seconds. In the aforementioned results, the reduced inertia constants can only decrease the converging time, making the system reach a new steady state quicker, and it has no effects on steady-state values.
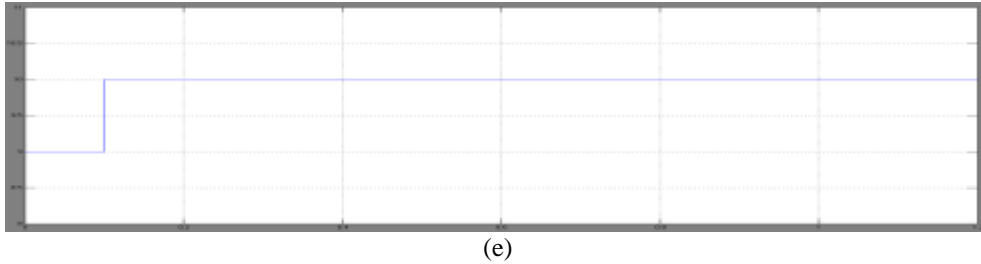

(a)

(b)

(c)

(d)

(e)

Fig-12: Wind step response. (a) DC-link voltage Vdc. (b) Rotor speed ω_r. (c) Active power P. (d) Reactive power Q. (e) Wind speed v_w

At last, the system dynamic response to a grid disturbance is investigated. At Vw=9m/s, a remote voltage droop in grid is programmed from t=0.09to 0.29 s. The dynamic responses represented in Fig. 15. During this process, since the wind speed remains the same, control system effectively makes the system recovers in approximate 0.1 s.

V. CONCLUSION

This paper has discussed of the wind turbine system using DFIG generator system. With the DFIG wind power system is modelled and simulated in Matlab/Simulink. An optimal active-power-versus-rotor-speed relationship has been proposed for turbine model first, and it functions as a lookup table for tracking the maximum output active power.

In contrast, the DFIG system does not need reactive power compensator to hold distribution line voltage and achieves optimal active power controlling. Both voltage control schemes for two converters consist of a current regulation part and a cross-coupling part. The turbine emulator system performs well and follows the theoretical and simulated maximum power extraction points in different operating conditions.

REFERENCES

[1] M. Orabi, T. Ahmed, and M. Nakaoka, "Efficient performances of induction generator for wind energy utilization," inProc. 30th Annu. Conf. IEEE Ind. Elect. Soc., Nov. 2004, pp. 838–843.

[2] M. Molinas, J. A. Suul, and T. Undeland, "Low voltage ride through of wind farms with cage generators: STATCOM versus SVC,"IEEE Trans. Power Electron., vol. 23, no. 3, pp. 1104–1117, May 2008.

[3] Z. Chen, J. M. Guerrero, and F. Blaabjerg, "A review of the state of the art of power electronics for wind turbines,"IEEE Trans. Power Electron., vol. 24, no. 8, pp. 1859–1875, Aug. 2009.

[4] Y. Lei, A. Mullane, and G. Lightbody, "Modeling of the wind turbine with a doubly fed induction generator for grid integration studies,"IEEE Trans. Energy Convers., vol. 21, no. 1, pp. 257–264, Mar. 2006.

[5] R. Ganon, G. Sybille, and S. Bernard, "Modeling and real-time simulation of a doubly-fed induction generator driven by a wind turbine," presented at the Int. Conf. Power Systems Transients, Montreal, QC, Canada, Jun. 2005, Paper IPST05-162.

[6] H. Sun, Y. Ren, and H. Li, "DFIG wind power generation based on backto-back PWM converter," in Proc. IEEE Int. Conf. Mechatron. Autom., Aug. 2009, pp. 2276–2280.

[7] L. Xu and P. Cartwright, "Direct active and reactive power control of DFIG for wind energy generation,"IEEE Trans. Energy Convers., vol. 21, no. 3, pp. 750–758, Sep. 2006.

[8] S. Heier, Grid Integration of Wind Energy Conversion Systems. Hoboken, NJ, USA: Wiley, 2006.

[9] N. W. Miller, W. W. Price, and J. J. Sanchez-Gasca, "Dynamic modelling of GE 1.5 And 3.6 wind turbine-generators," GE Power Systems Energy Consulting, Gen. Elect. Int., Inc., Schenectady, NY, USA, Oct. 2003.

[10] R. Pena, J. C. Clare, and G. M. Asher, "Doubly fed induction generator using back-to-back PWM converters and its application to variable-speed wind-energy generation,"Proc. Inst. Elect. Eng.—Elect. Power Appl., vol. 143, no. 3, pp. 231–241, May 1996.

[11] Feijoo, J. Cidras, and C. Carrillo, "Third order model for the doubly-fed induction machine," Elect. Power Syst. Res., vol. 56, no. 2, pp. 121–127, Nov. 2000.

[12] T. Ghennam, E. M. Berkouk, and B. Francois, "DC-link voltage balancing algorithm using a space-vector hysteresis current control for three-level VSI applied for wind conversion system," inProc. Power Elect. Appl. Eur. Conf., Sep. 2007, pp. 1–10.

[13] M. Stiebler,Wind Energy Systems for Electric Power Generation. Berlin, Germany: Springer-Verlag, 2008